Theoretical Notes

Note 197

November 1973

PROPAGATED EMP FROM TANGENT AND BURIED BURSTS

Captain James E. Brau
Major Gregory H. Canavan
Captain Leon A. Wittwer
Lt Arthur E. Greene

Air Force Weapons Laboratory
Kirtland Air Force Base, New Mexico

ABSTRACT

Calculations describing the ionospheric propagation of high-altitude electromagnetic pulses (EMP) to satellite altitudes are reported. Both tangent and buried burst scenarios are treated. The calculations are based on the AFWL CHEMP code for self-consistent calculations of radiated EMP, modified by the inclusion of a swarm treatment of secondary and ionospheric electrons. The region of applicability of this swarm treatment has been determined by a separate Monte Carlo calculation. By carrying the calculations all the way from the burst point through the E region, we are able to account fully for the D region heating, the increased absorption and cascading it produces, and the increased cutoff frequency which results. The code calculations are evaluated for sensitivity to the ambient ionospheres used.

CONTENTS

ILLUSTRATIONS

SECTION I

INTRODUCTION

The calculation presented is of the ionospheric propagation of electromagnetic pulses (EMP) from tangent and buried bursts which treat explicitly the nonlinear effects of heating and cascading ignored in previous solutions (ref. 1). Tangent bursts are events in which the gammas directed just above the earth's limb produce a radiated electromagnetic pulse which propagates out through the ionosphere on the other point of tangency. Buried bursts, on the other hand, result from lower-altitude detonations (between 20 and 80 kilometers) in which the upward-directed gammas interact with low density air, likewise resulting in an ionospherically propagated EMP with a large angular coverage.

SECTION II

MODEL

The tangent pulses injected into the ionosphere at 55-km altitude were generated by CHEMP, a self-consistent particle code described in a companion report (ref. 2). The fields were propagated through the ionosphere according to the theory of Karzas and Latter (refs. 3 and 4) and Longmire (ref. 5).

$$\frac{\partial E(T)}{\partial r} = -\frac{E(T)}{r} - \frac{2\pi}{c} J(T), \quad T = t - \frac{r}{c} \tag{1}$$

where the current density is defined by the characteristics of the local swarm $J(T) = -en(T)v(T)$. The electron number density, n, and the electron drift velocity, v, were determined by employing the swarm model of reference 6. By assuming the swarm to be in equilibrium with a mean electron energy of 3U/2, one can describe its characteristics with the swarm equations (ref. 6)

$$\frac{dn}{dt} = C(U)n \tag{2}$$

$$\frac{dU}{dt} = -\frac{2}{3}\frac{evE}{1.6\times10^{-12}} - g(U)(U-U_o) - \frac{U}{n}\frac{dn}{dt} - \frac{10}{n}\frac{dn}{dt} \tag{3}$$

$$\frac{dv}{dt} = -\frac{eE}{m} - f(U)v - \frac{v}{n}\frac{dn}{dt} \tag{4}$$

where the cascade rate, C(U), and the momentum and energy transfer collision frequencies, f(U) and g(U), are given as analytic functions (ref. 6) of U, as follows:

$$\frac{C(U)}{N}\left(\frac{cm^3}{sec}\right) = \frac{3.3\times10^{-14}\ U^{8.7}}{(1+5.87\times10^{-3}U^{5.5})(1+1.29\times10^{-3}U^{3.2})} + 3.26\times10^{-7}\ \exp\ (-44.08/U)$$

$$\frac{f(U)}{N}\left(\frac{cm^3}{sec}\right) = \frac{1.25\times10^{-7}U^{0.935}}{(1+1.26U^{1.67})^{0.373}}$$

SECTION III

TANGENT BURSTS

Figure 1 compares the Fourier transform of the injected pulse with the Fourier transform of the transmitted pulse from a 10-kt gamma burst at 100 km propagated through the D region of the nighttime sunspot minimum ionosphere (A, hereafter referred to as the standard) and the daytime sunspot maximum ionosphere (B). The injected pulse contained 5.4 millijoule/meter^2, of which 0.29 mj/m^2 (0.11 mj/m^2) propagated through the nighttime (daytime) ionosphere, with a reduction of 30 percent (70 percent) in the Fourier amplitudes at 60 MHz and a factor of 4(10) at 20 MHz.

Figure 2 shows the energy absorbed by the ionosphere, $\int dt \underline{J} \cdot \underline{E}$, as a function of altitude for the standard calculation A. The maximum deposition occurs around 85 km with a secondary enhancement around 75 km. Figure 3 shows that the higher peak corresponds to the maximum heating; the electron energy U, and with it the collision frequencies, has been enhanced by three orders of magnitude. It also shows that the lower altitude enhancement is coincident with less heating but much more cascading due to the faster ionization rates in the denser air. Note that due to the ubiquitous, strong heating, analytic investigations of ionospheric nonlinearities (appendix I) can be quantitatively misleading if based on collision frequencies appropriate for the ambient ionosphere (ref. 1). To predict even the qualitative, let alone the quantitative, features seen in code calculations, analytic estimates must be based on collision frequencies in the heated ionosphere (appendix II).

The sensitivity of these predictions of EMP transmission to the ambient ionosphere below 90 km, the region of maximum absorption, has been assessed through parametric studies in which the electron density above 90 km is kept constant and the ambient electron density at lower altitudes is varied by changing A in the equation

$$n = 10^3 \exp(A(h-90)), \quad h \leq 90 \text{ km} \tag{7}$$

Figure 4 presents the results of these parametric calculations. Curve A which corresponds to the standard nighttime minimum ionosphere with A = 0.23/km

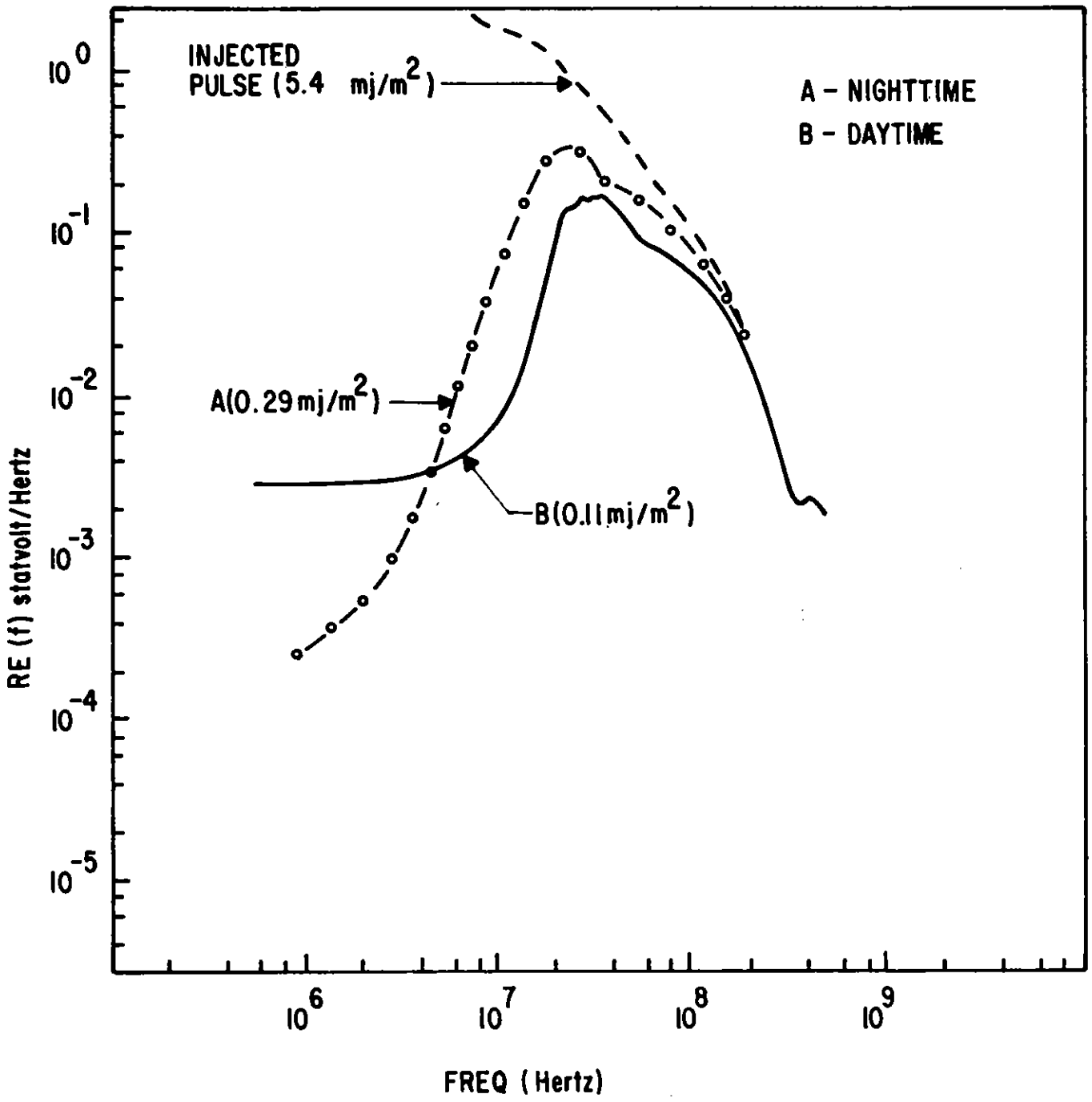

Figure 1. The Fourier Transform of the Injected EMP from a 10-kt Gamma Source at 100 km and of the Pulses Transmitted through the Nighttime A and Daytime B Ionospheres.

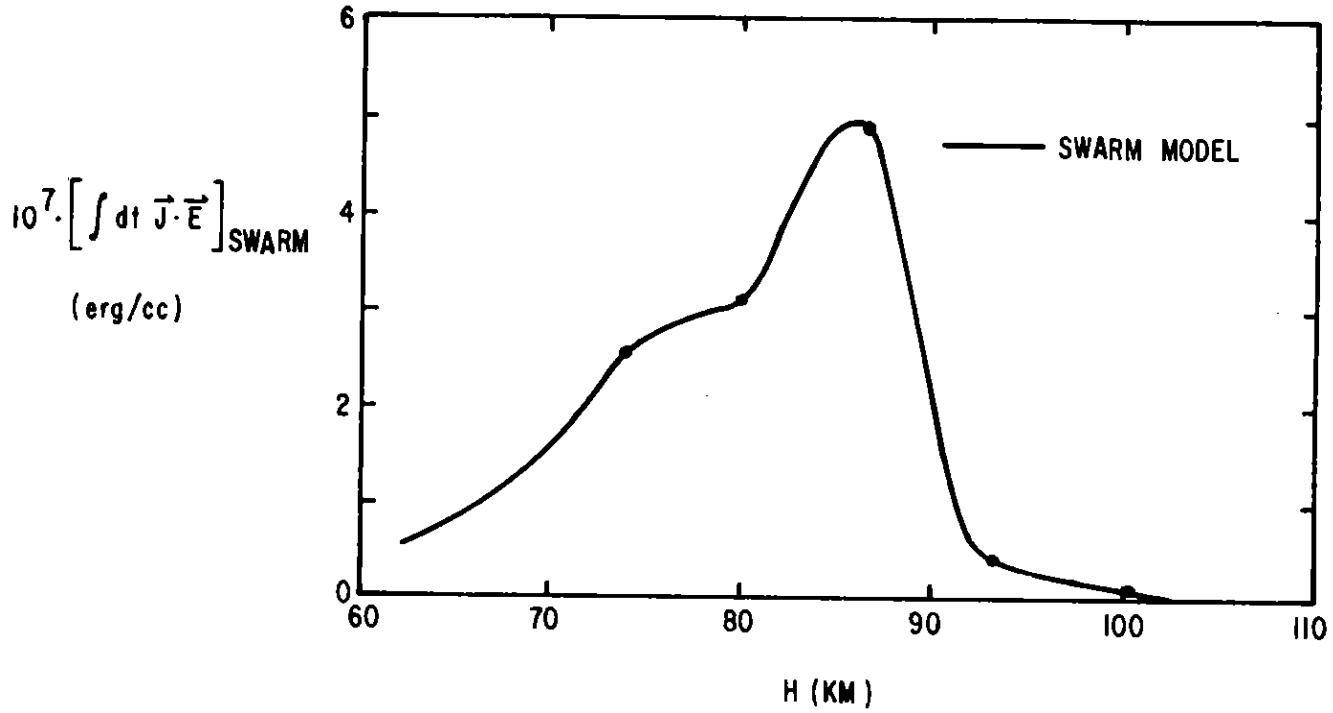

Figure 2. The Energy Deposition Versus Altitude for Case A of Figure 1.

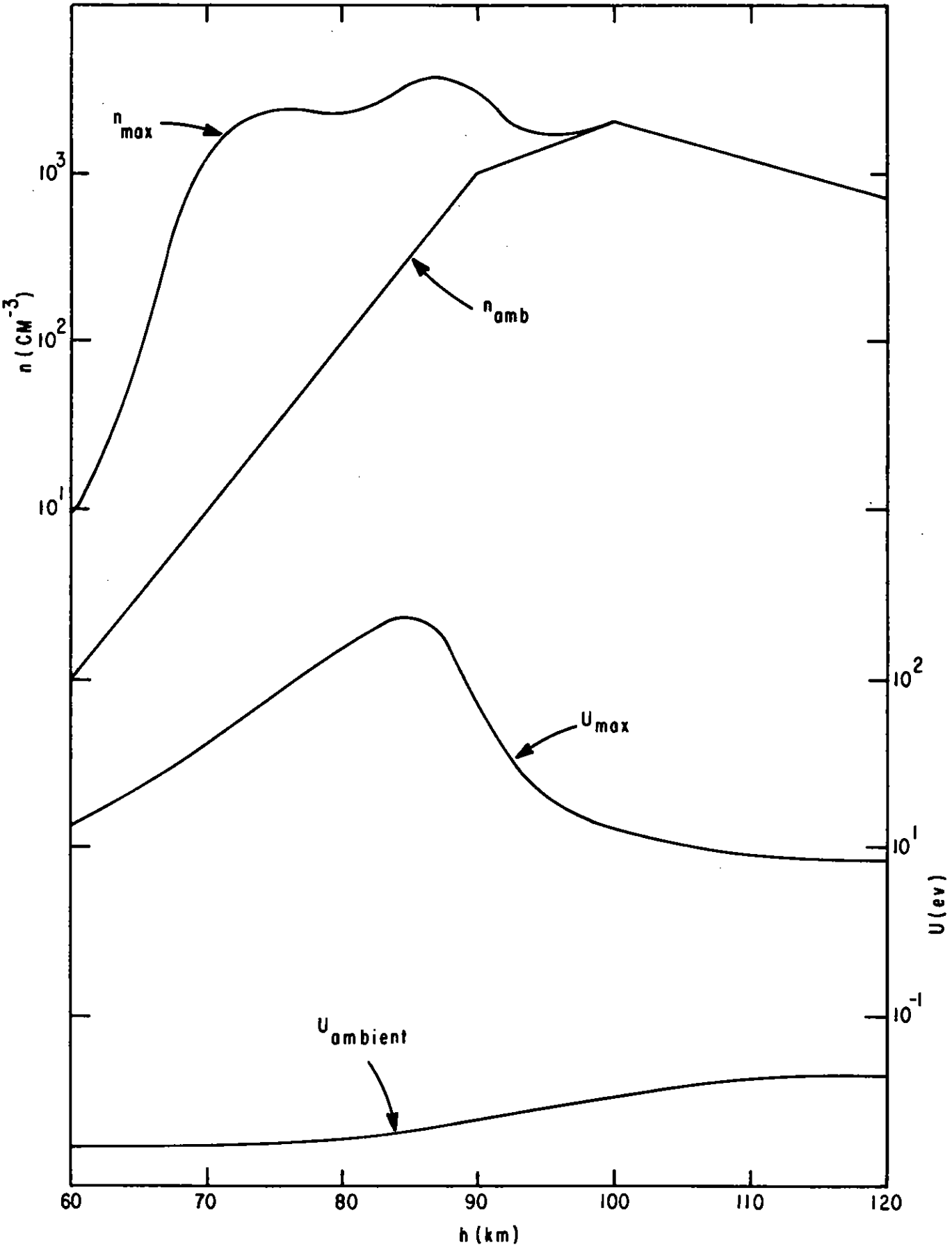

Figure 3. The Ambient and Maximum Values of Electron Number Density and Electron Temperature Versus Altitude for Case A of Figure 1.

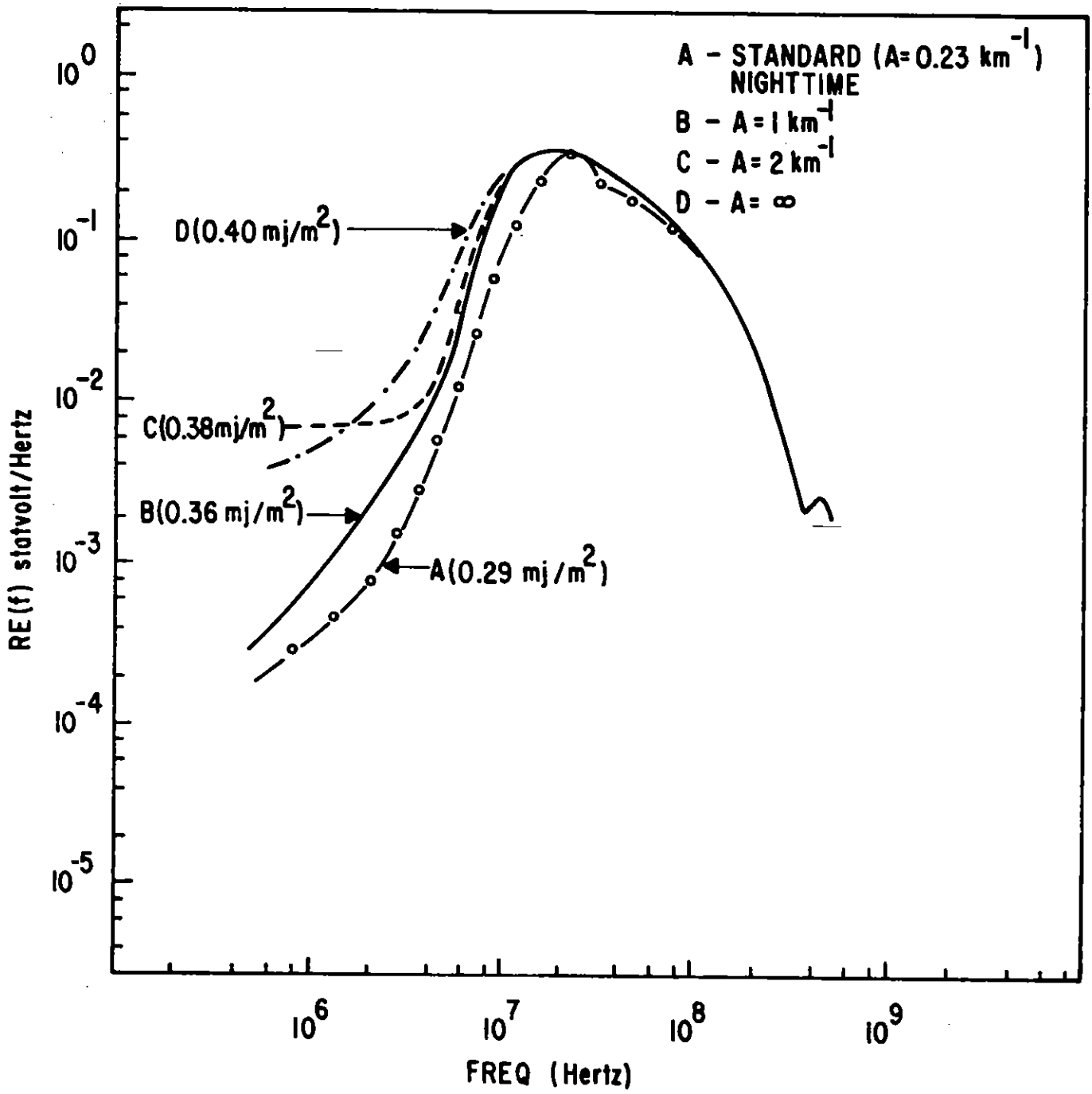

Figure 4. The Fourier Transforms of the Transmitted Pulse through the Nighttime Ionosphere with A = 0.23/km, 1/km, 2/km, and ∞/km.

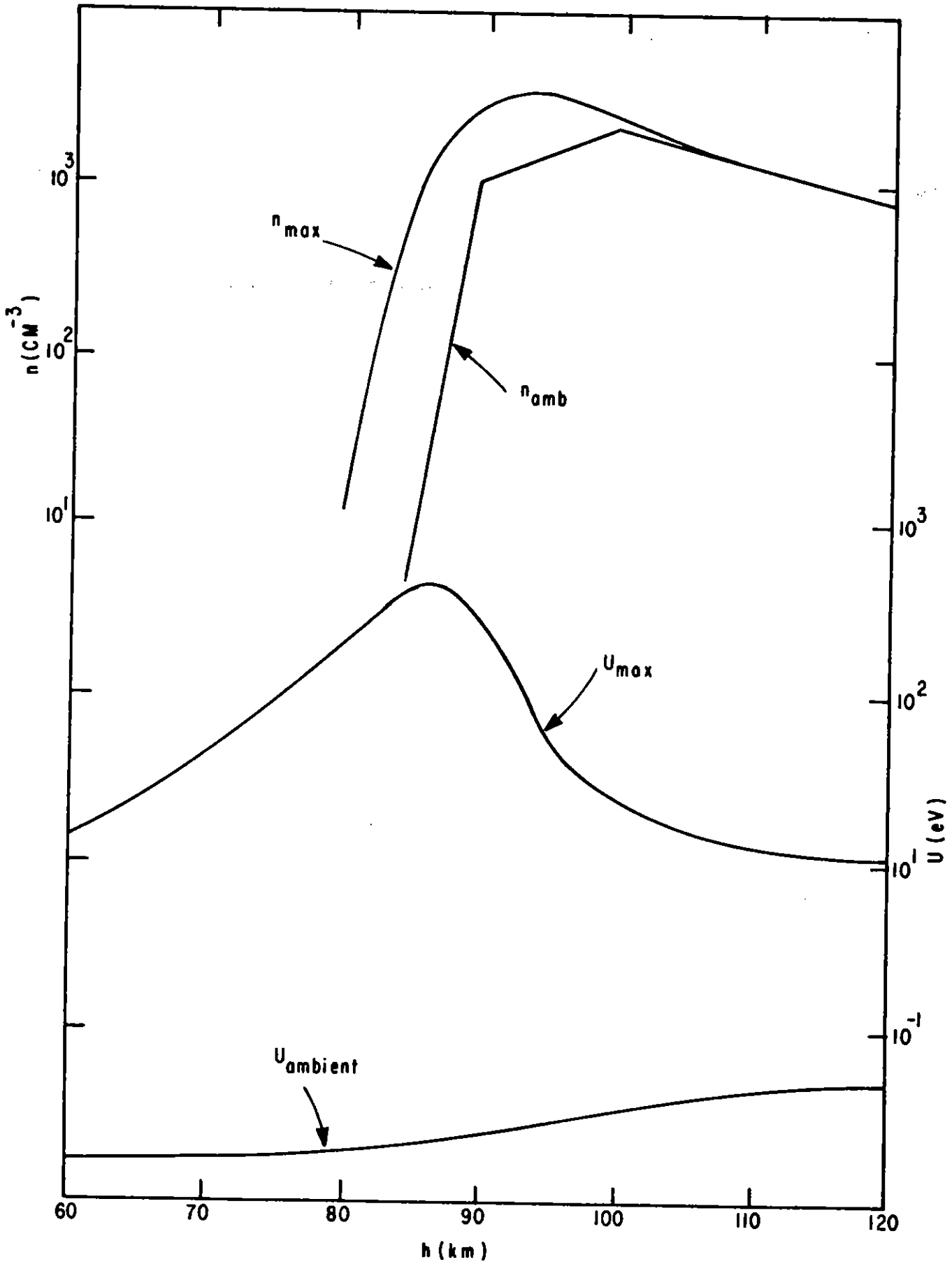

Figure 5. The Ambient and Maximum Values of Electron Number Density and Electron Temperature Versus Altitude for A = 1/km in Equation 7.

displays a notch at about 20 MHz owing to preferential absorption of those frequencies due to cascade-enhanced absorption around 70 km. Curve B shows that increasing A to 1/km reduces the ambient electron number density in that region to such low values that even the cascade absorption is insignificant, removing the structure above 20 MHz and increasing the transmitted fluence by 20 percent. Comparing figure 5 with figure 3 indicates that depleting the lower ionosphere negates the cascade-enhanced absorption at lower altitudes and shifts the heating peak to higher altitudes. Increasing A further changes the transmission little; curve D with $A = \infty$ which corresponds to removing all electrons below 90 km differs little from B.

SECTION IV

MONTE CARLO CALCULATIONS

Note that the temperatures reached in figures 3 and 5 are several hundred eV, far beyond the energies for which the swarm model of reference 6 is intended. It has, therefore, been extended by developing a Monte Carlo model of the interaction of a finite sample ($\approx 10^3$) of electrons with neutral nitrogen molecules. By solving the equations of motion for each electron in the sample including acceleration by the applied EM pulse, elastic, and inelastic collisions, and logging the results it was determined explicitly the electron distribution function at each instant, which was used to determine the sensitivity of the results above to the assumption (ref. 6) that the collision frequencies at any instant are those appropriate for the equilibrium distribution function at the instantaneous value of U. In these calculations the momentum transfer cross sections below 10 eV were taken from Engelhardt et al. (ref. 10) and those above from Shyn et al. (ref. 11). The nonionizing inelastic cross sections were taken from reference 10, and the ionization cross section was taken from Rapp and Englander-Golden (ref. 12). During a time step, Δt, a particle velocity changes by $\Delta v = \frac{eE}{m} \Delta t$, the probability of a collision is $1 - e^{-n\sigma(v)v\Delta t}$, and in the event of a collision, the final particle velocity, v, is related to the initial particle velocity, v^1, by (1) $v^2 = v^{12}$ for an elastic collision, (2) $v^2 = v^{12} - v_x^2$ for an exciting collision, and (3) $v^2 = 1/2)v^{12} - v_i^2)$ for an ionizing collision (ref. 13).

The pulses obtained from the standard calculation above were applied to the Monte Carlo to assess the accuracy of the swarm model. To this end one defines the ratio R = the energy deposited in the Monte Carlo calculations divided by the energy deposited in the swarm model calculation. The computed values of R at several altitudes are:

H(km)	74	80	86	93	100
R	6.9	2.2	1.02	0.90	1.01

Below 80 km the disagreement is most pronounced, amounting to a factor of 7 underestimate of the absorption at 74 km by the simple swarm model. These discrepancies may be attributed to two factors: nonequilibrium distributions and

poor fits to cascading rates and collision frequencies at high energies. The latter source has been eliminated by simulating the swarm experiments of Phelps and collaborators at higher values of E/N and using the results to improve fits. When the distribution comes into equilibrium at a given value of E/N, equations 3 and 4 show that the new fits are given by

$$g(U) + \frac{1}{n}\frac{dn}{dt}\left(1 + \frac{10}{U}\right) = -\frac{evE}{2.4\times10^{-12}(U-U_o)} \tag{8}$$

$$f(U) + \frac{1}{n}\frac{dn}{dt} = -\frac{eE}{mv} \tag{9}$$

These frequencies were determined as functions of mean energy, not characteristic energy; the new fits of figure 6 were then used in the swarm model

$$\frac{dU}{dt} = \frac{-evE}{2.4\times10^{-12}} - \left(g(U) + \frac{1}{n}\frac{dn}{dt}\right)(U-U_o) - \frac{10}{n}\frac{dn}{dt}$$

$$\frac{dv}{dt} = -\frac{eE}{m} - \left(f(U) + \frac{1}{n}\frac{dn}{dt}\right)v$$

The ratio R of the Monte Carlo deposition to the swarm model deposition for these new fits.

H(km)	74	80	86	93	100
R(new fits)	0.68	0.76	1.00	1.01	0.99

The lower altitudes still show the largest discrepancies, but they have been significantly reduced. The swarm model now overestimates the absorption at these altitudes by about 30 percent, which is attributed to the swarm model's assumption of an equilibrium distribution. Figure 7 compares the transmitted Fourier transform with the new fits to that from a calculation done with the old fits. The transmitted energy has been increased by over 50 percent as have the maximum amplitudes around 20 MHz. Owing to the good agreement shown in the above chart it is felt that the model dependencies of curve B are small compared to uncertainties in the ambient ionosphere.

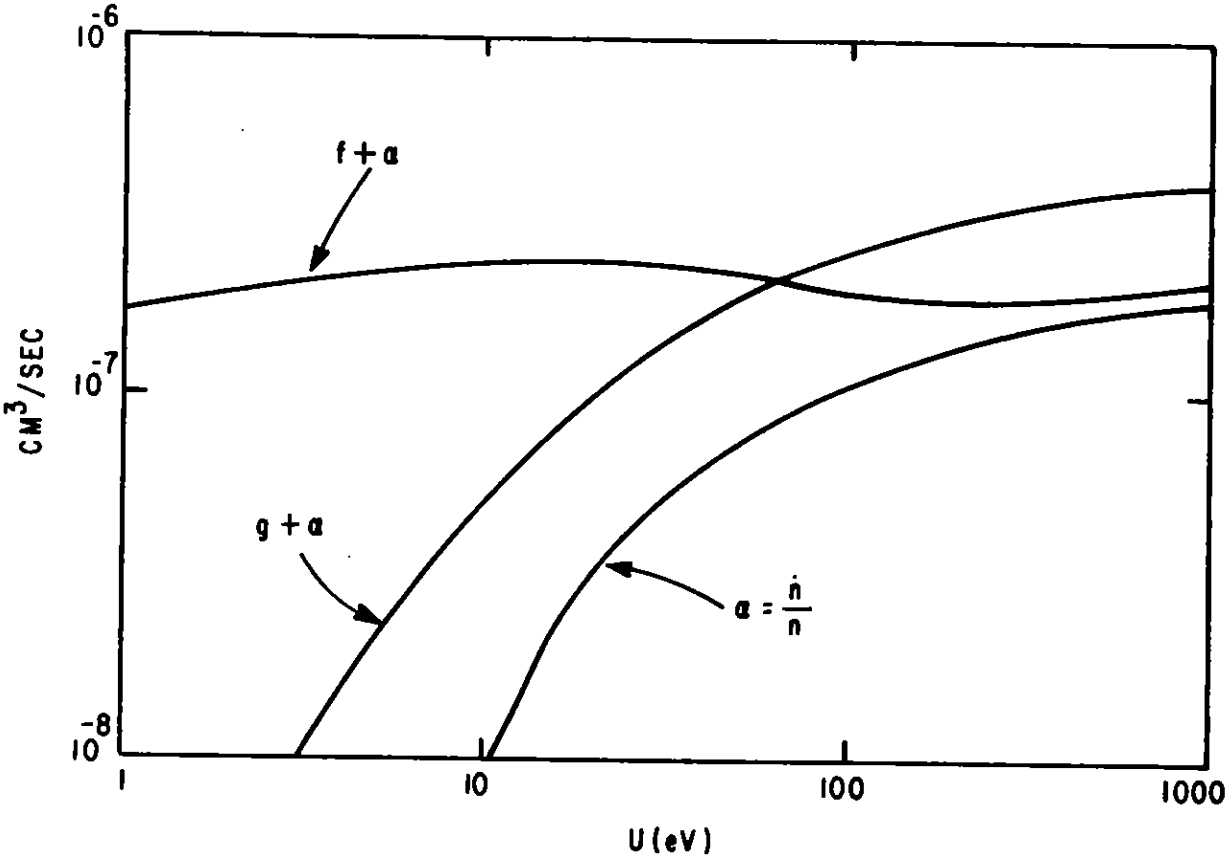

Figure 6. The Electron-neutral Collision Frequencies and Cascading Rate as a Function of Mean Electron Energy as Determined by the Electron Monte Carlo Calculations.

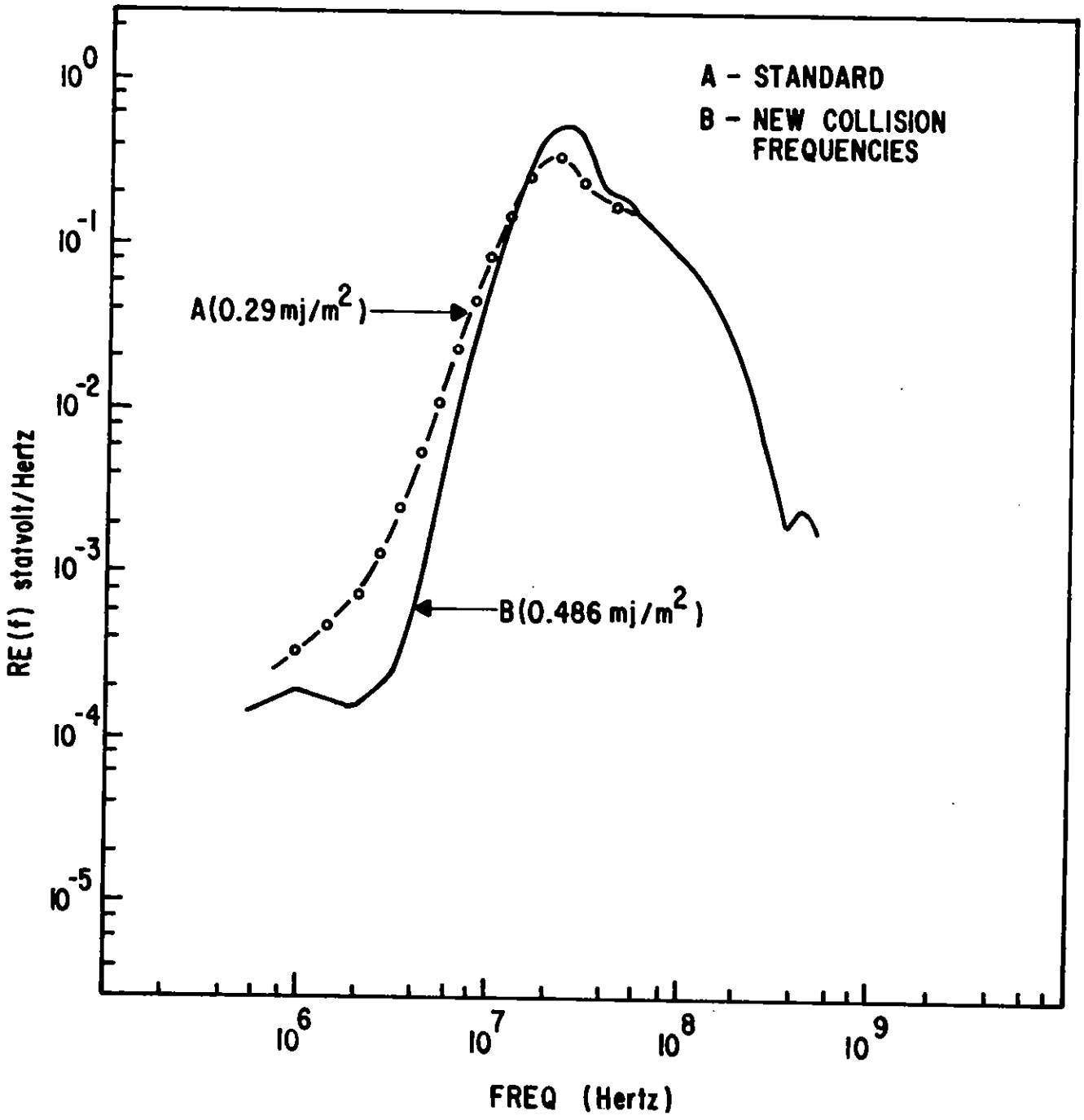

Figure 7. The Fourier Transforms of Case A of Figure 1 Where the Electron Collision Frequencies and Cascading Rate Have Been Defined in Reference 6 and Is Shown in Figure 6.

SECTION V

BURIED BURSTS

The CHEMP-generated fields seen by an observer at 115 km from buried bursts at 35, 50, and 65 km are shown in figure 8. In general as the burst altitude goes from 35 to 65 km, the amplitude increases and the proportion of high-frequency content decreases. The R·E product of the first peak, to within 12 percent, is 3.51×10^6 statvolts for all three bursts.

Figure 9 displays the Fourier transform of the 50-km burst. The R·E(w) product at about 10 MHz is about 6.5×10^{-2} statvolts/Hz. Satellites below 300 km will see all of the spectrum. Above 300 km, the spectrum is cut off at about 4 MHz by the plasma frequency.

The R·E product-derived Fourier spectrum in figure 9 can be considered as an extreme worst case for buried bursts. This conclusion is based on the large yield, the source treatment, and the insensitivity of the R·E product with altitude for a given yield.

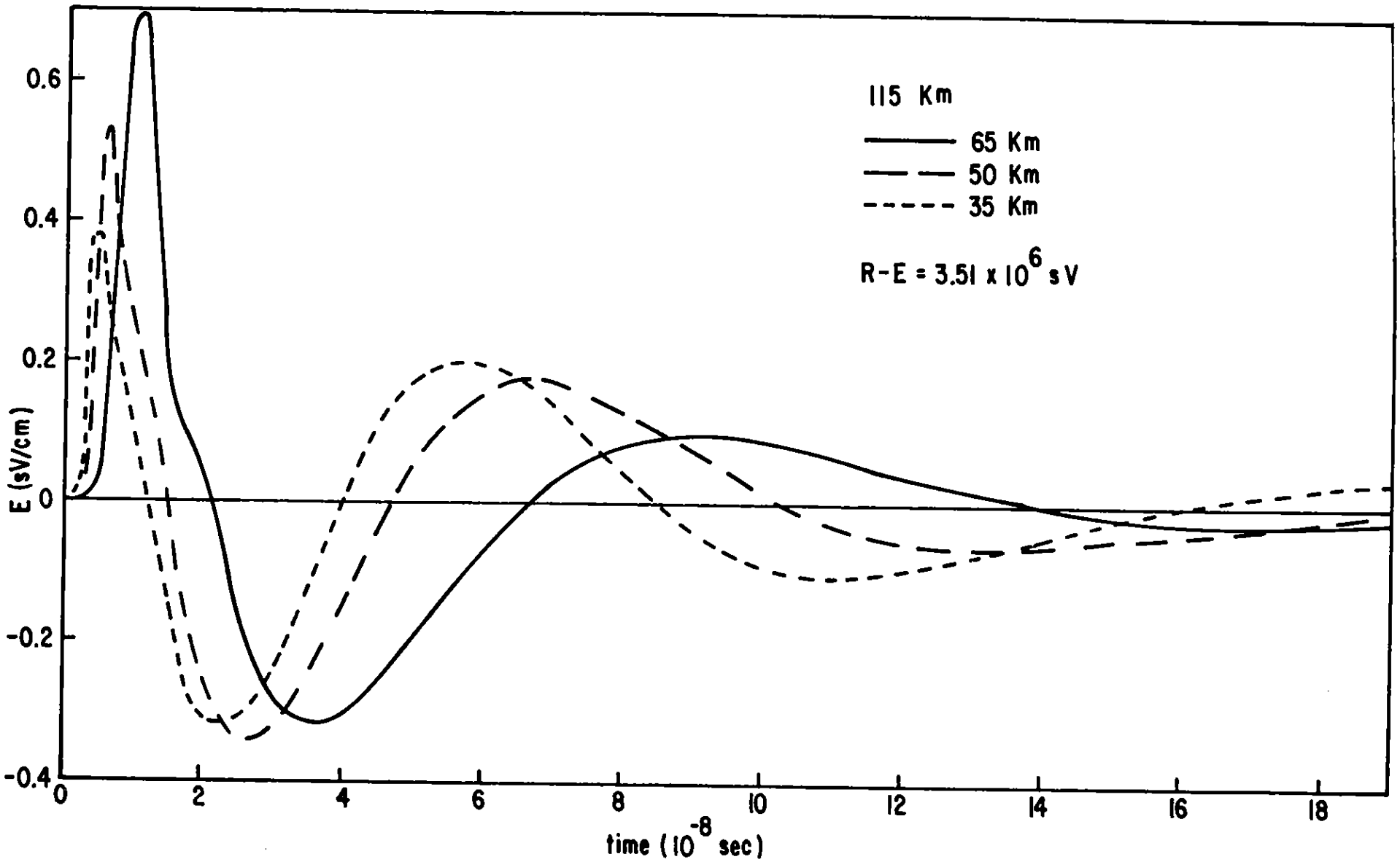

Figure 8. Time-dependent Field at 115 km from Buried Bursts at 65 km, 50 km, and 35 km.

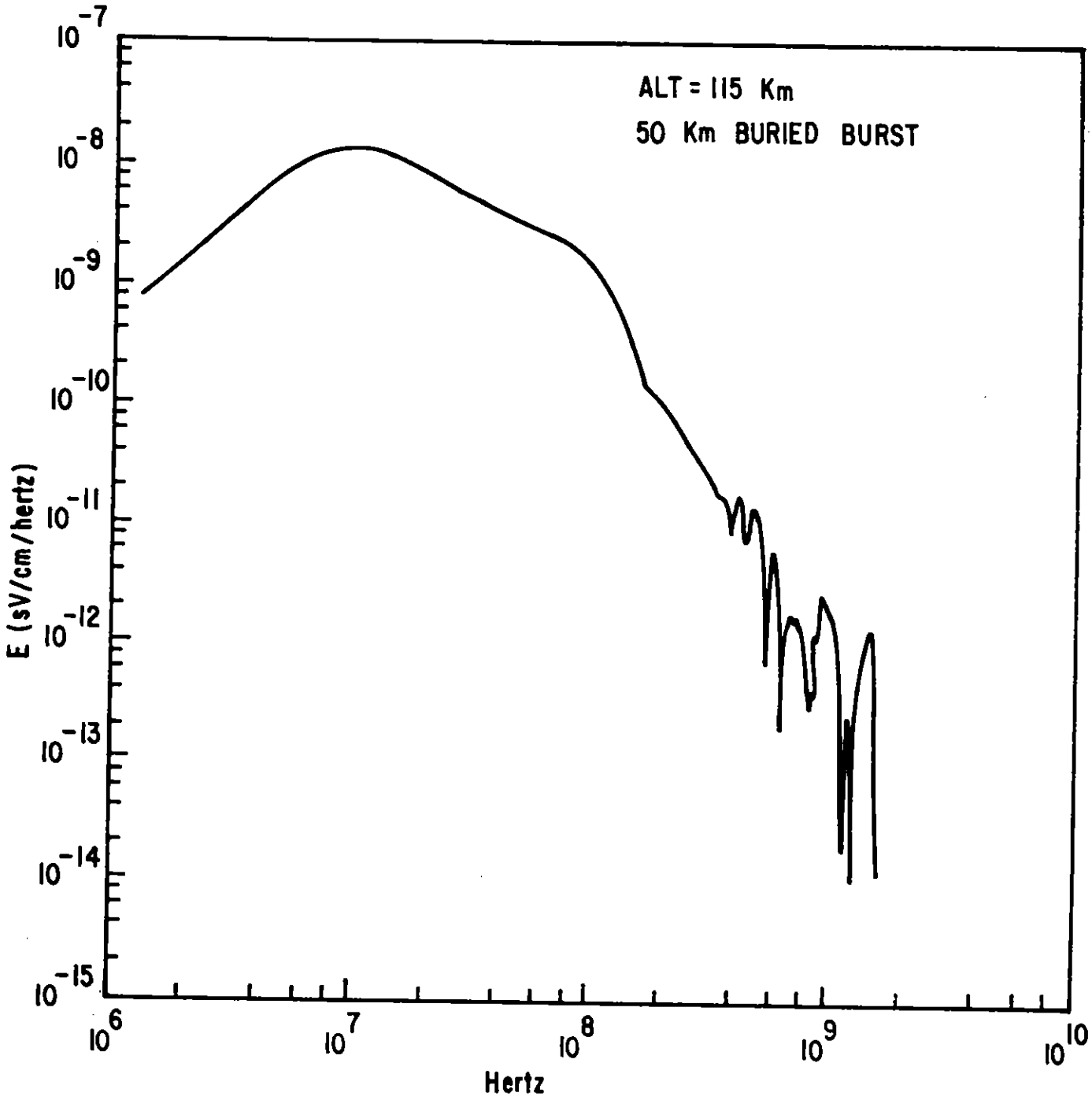

Figure 9. Fourier Transform of Field from Buried Burst at 50 km.

APPENDIX I

SEPARATION OF NONLINEAR AND LINEAR EFFECTS ON PROPAGATED EMP

An upward propagating pulse with Fourier coefficients $E_i(w)$ at 50 km heats the $n(cm^{-3})$ free electrons at altitude z to an energy (ref. 14)

$$U(z) = n^{-1} \int_W^\infty dw\ K(w,z)(c|E_i(w)|^2/4\pi)\ \exp\left(-2\int_0^z dz' K(w,z')\right) \qquad (10)$$

where $K(w,z) = p^2 f/c(f^2 + w^2)$ is the microwave absorption coefficient, f is the momentum transfer collision frequency between electrons and neutral molecules, and $p^2 = 4\pi ne^2/m$ is the square of the electron plasma frequency. Since $\overline{nf} \approx nf = 10^9/cm^3\text{-sec}$ between 50 and 150 km in the daytime, $K \approx 4\pi e^2 nf/mc(f^2 + w^2) \equiv A/(f^2 + w^2)$. In the high-frequency approximation (ref. 14)

$$Y(w,z) = 2\int_0^z dz' K(w,z') \approx 2Az/w^2, \text{ for } w^2 >> f^2 \qquad (11)$$

Note that contributions from frequencies for which $Y(w,z) \geq 1$ are effectively truncated from equation 10, so that the choice of cut-off frequency

$$W = (2Az)^{1/2} \qquad (12)$$

allows equation 10, to be simplified to

$$U(z) = n^{-1} \int_W^\infty dw\ e^2 \overline{nf} |E_i(w)|^2/mw^2 \qquad (13)$$

Since $W >> p$ for $z < 130$ km, reflection need not be considered below that altitude. Note also that W is everywhere $>> b = 4\times10^6$ rad/sec, the smaller frequency characterizing a double exponential $E_i(w)$, so that $E_i \approx E/w$, and equation 13 further simplifies to

$$U(z) \approx e^2\ f\ E^2/3mW^3 \qquad (14)$$

A disturbing aspect of equation 14 is the prediction that electron heating increases exponentially with decreasing altitude. That this result is merely an artifact of an inappropriate use of the high-frequency approximation can be

shown by a simple calculation which breaks the heating into integrals over low and high frequency components

$$U = U_l + U_h = \int_p^f dU + \int_f^\infty dU \tag{15}$$

In U_l, $K \approx A/f^2$, $Y \approx \exp(-AH/f^2)$, where $H \approx 8$ km is the atmospheric scale height, so that U_l reduces to

$$U_l = (AcE^2 \exp(-AH/f^2)/4\pi nf^2) \int_p^f dw/(b + w)^2 \approx AcE^2/4\pi f^2 b,\ z < 60 \text{ km} \tag{16}$$

and $U_l \approx 0$ higher where $AH/f^2 >> 1$. In U_h, $K_2 \approx A/w^2$ and $Y \approx \exp(-2Az/w^2)$, so that $U_h = AcE^2/4\pi nf^3$ for $z < 60$, and $U_h \approx AcE^2/n4\pi(Az)^{3/2}$ higher. Adding U_l and U_h one finds

$$U = \begin{cases} e^2E^2/mfb & z < 60 \\ e^2E^2f/m(Az)^{3/2} & z > 60 \end{cases} \tag{15}$$

which clearly shows that heating falls off exponentially below 60 km as well as above. It also shows that $U(z < 60)$ scales as $1/b$ due to the low-frequency contributions ignored in equation 14.

APPENDIX II

HIGHER CUTOFF FREQUENCY DUE TO IONOSPHERIC HEATING

The integral $Y(w,z)$ (appendix I, equation 11) which determines the thickness of the ionosphere up to altitude z at frequency w can be evaluated by breaking it into low ($w < f$) and high ($w > f$) frequency parts

$$Y(w,z) = Y_l + Y_h = \int_0^{z_w} dY + \int_{z_w}^{z} dY, \quad f(z_w) = w \tag{18}$$

Approximate $K = A/(f^2 + w^2)$ as in appendix I to evaluate $Y_l(z < z_w) = AH/f^2$ and $Y_l(z > z_w) = AH/w^2$, while $Y_h(z < z_w) = 0$ and $Y_h(Z > z_w) = 2A(z - z_w)/w^2$. Combine these results to obtain $Y(z < z_w) = AH/f^2$ and $Y = (z > z_w) = A(H + 2(z - z_w))/w^2$. Clearly, all low frequencies, i.e., those for which $w < w_a = (AH)^{1/2}$, will be strongly absorbed below z at an altitude z_a where $Y(w,z) = 1$. Since $Y(z < z_w) = AH/f^2$ and $f = f_o \exp(z_o - z)/H$

$$z_a = (H/2)\ln(f_o^2/AH) \tag{19}$$

For $f_o = 6_7$/sec at $z_o = 50$ km and $A = 4_7$/sec^2-cm, $z_a = 65$ km in rough accord with equation 17 of appendix I. The cutoff frequency W of that note, is defined more precisely as the frequency at which $Y(w,z_m) = 1$ where $z_m = 150$ km is the altitude at which the product nf in the numerator of K begins its rapid fall, truncating the integrals in equation 18 abruptly. For the values above, $W = (2A(z_m - z_o))^{1/2} = 3_7$/sec, while $w_a = 6_6$/sec.

The above results can be used to evaluate the effect of the strong heating predicted by equation 17 of appendix I. Raising the electrons to 1 to 10 eV increases f by about 100 which also increases A by a like amount. According to equation 19 this raises z_a to 80 km and increases w_a and W by 10.

REFERENCES

1. Messier, M. A., "The Ionospherically Propagated Exoatmospheric EMP Environment," EMP Theoretical Note 163, 25 January 1972.

2. Wittwer, L. A., Brau, J. E., and Canavan, G. H., CHEMP: A Code for Self-Consistent Calculations of High Altitude EMP, Theoretical Note 198, March 1974.

3. Karzas, W. J. and Latter, R., "Electromagnetic Radiation from a Nuclear Explosion in Space," EMP Theoretical Note 27, October 1961.

4. Karzas, W. J., Latter, R., "Detection of the Electromagnetic Radiation from Nuclear Explosions in Space," EMP Theoretical Note 40, October 1964.

5. Longmire, C. L., "Electromagnetic Fields Produced by Nuclear Explosions," Journal of Missile Defense Research, Summer 1965.

6. Higgins, D. F., Longmire, C. L., and O'Dell, A. A., A Method for Estimating the X-ray Produced Electromagnetic Pulse Observed in the Source Region of a High-Altitude Burst, Theoretical Note 181, February 1973.

7. Phelps, A. V. and Kasner, W. H., Studies and Experimental Work on Atomic Collision Processes Occurring in Atmospheric Gases, AFWL-TR-66-34, Air Force Weapons Laboratory, Kirtland AFB, NM, May 1966.

8. DASA Reaction Handbook, Chapter 9, July 1967.

9. Frost, L. S., and Phelps, A. V., "Rotational Excitation and Momentum Transfer Cross Sections for Electrons in H and N from Transport Coefficients," Physical Review, 127, 1621, 1963.

10. Engelhardt, A. G., Phelps, A. V., and Risk, C. G., "Determination of Momentum Transfer and Inelastic Collision Cross Sections for Electrons in Nitrogen Using Transport Coefficients," Physical Review, 135A, 1566, 1964.

11. Shyn, T. W., Stolarski, R. S., and Carigan, G. R., "Angular Distribution of Electrons Elastically Scattered from N_2," Physical Review, 6A, 1002, 1972.

12. Rapp, D. and Englander-Golden, D., "Total Cross Sections for Ionization and Attachment in Gases by Electron Impact. I. Positive Ionization," Journal of Chem Phys, 43, 1464, 1965.

13. Kline, L. E. and Siambis, J. S., "Computer Simulation of Electrical Breakdown in Gases; Avalanche and Streamer Formation," Physical Review, 5A, 794, 1972.

14. Messier, M. A., A First Look at the Importance of Non-Linear Effects in Determining Propagated Satellite EMP Criteria, MRC Note, 27 April 1973.